Energy Balance in Medium-Scale Methanol, Ethanol, and Acetone Pool Fires

Sung Chan Kim,* Ki Yong Lee,** and Anthony Hamins

National Institute of Standards and Technology, Gaithersburg, MD 20899 USA[*]

ABSTRACT

Several series of measurements were made to characterize medium-scale pool fires steadily burning in a well-ventilated, quiescent, open environment. Time-averaged local measurements of radiative and total heat flux were made in steadily burning methyl alcohol (methanol; CH_3OH), ethyl alcohol (ethanol; C_2H_5OH), and acetone ($(CH_3)_2CO$) pool fires. The fuel lip height in a water-cooled stainless-steel burner was maintained at 10 mm. Schmidt-Boelter heat flux gauges were used to measure the radiative emission to the surroundings. The total heat flux directed towards the pool surface was measured using a Gardon gauge positioned just above the pool surface. A previously developed method was used to calculate the convective heat flux to the pool surface, allowing estimation of the radiative flux, which agreed within experimental uncertainty with a previous measurement in the methanol pool fire. The steady-state mass burning rate was measured using a load cell, and the heat release rate was measured in the exhaust using calorimetry. The energy balance for each of the fires was determined. The results showed that both radiation and convection play significant roles in these pool fires. Radiation was the dominant mechanism of heat feedback to the fuel surface, accounting from 68 % to 88 % of the energy, while enthalpy convected in the plume represented 68 % to 78 % of the fire's total energy, far exceeding radiative emission to the surroundings.

KEYWORDS: burning rate, energy balance, pool fires, radiative flux

permanent addresses:
* *Kyungil University, Gyeongbuk, South Korea*
** *Andong National University, Andong, South Korea*

[*] This research did not receive any specific grant from funding agencies in the public, commercial, or not-for-profit sectors.

1. INTRODUCTION

Use of fire modeling in fire protection engineering has increased dramatically during the last decade due to the development of practical computational tools and the decreased cost of computational power. Today, fire protection engineers use zone and field fire models like the Consolidated Fire and Smoke Transport Model (CFAST) and the Fire Dynamics Simulator (FDS) to provide fire safety design for buildings, nuclear power plants, aircraft cabins, trains, marine vessels among other types of applications [1, 2].* To be reliable, models require validation, which involves a large collection of experimental measurements. The objectives of this investigation were to provide experimental data on a well-defined configuration for use in fire model evaluation and to improve the general understanding of heat transfer pathways in medium-scale pool fires.

The focus of this study is the mass and heat transfer characteristics of medium-scale liquid pool fires steadily burning in a well-ventilated quiescent environment. A pool fire is a fundamental type of combustion phenomena in which the fuel surface is flat and horizontal, which provides a simple and well-defined configuration to test models and enhance the understanding of fire phenomena. In this study, methyl alcohol (methanol; CH_3OH), ethyl alcohol (ethanol; C_2H_5OH), and acetone ($(CH_3)_2CO$) were selected as fuels for investigation. Fires established using methanol are unusual as there is little or no carbonaceous soot present or emitted from the fire. Ethanol produces a fire with some amount of soot such that the fire's appearance is weakly yellow. Acetone produces a fire that has somewhat more soot.

Hu [3] and Joulain [4] provide overviews of the behavior of pool fires with an emphasis on fire physics. The rate of evaporation in a pool of burning liquid is controlled by heat transfer to the liquid pool, which is primarily controlled by gas-phase heat transfer processes involving convection and radiation. Thus, heat and mass transfer in a pool fire are coupled, and the mass burning rate ($\dot{m}$) of a pool fire depends on the total heat feedback to the pool surface ($\dot{Q}_s$).Consideration of the overall enthalpy balance about a control volume just above the liquid pool surface, encompassing the fire shows that the actual heat release rate ($\dot{Q}_a$) is equal to the sum of the energy radiated by the fire to the surroundings ($\dot{Q}_r$), the sensible enthalpy convected in the buoyant plume ($\dot{Q}_c$), heat feedback to the fuel surface ($\dot{Q}_s$), and losses to the burner ($\dot{Q}_b$):

$$\dot{Q}_a = \chi_a \dot{Q} = \dot{Q}_r + \dot{Q}_c + \dot{Q}_s + \dot{Q}_b \quad (1)$$

where the actual heat release rate is equal to the idealized or total heat release rate modified by the combustion efficiency (χ_a). Here, the total heat release rate ($\dot{Q}$) is defined as:

$$\dot{Q} = \dot{m}\, \Delta H_c \quad (2)$$

* Certain entities, equipment, or materials may be identified in this document in order to describe an experimental procedure or concept adequately. Such identification is not intended to imply recommendation or endorsement by the National Institute of Standards and Technology, nor is it intended to imply that the entities, materials, or equipment are necessarily the best available for the purpose.

where $\dot{m}$ is the mass vaporization rate and ΔH_c is the heat of combustion for a specific fuel.

Heat feedback from a fire to its fuel surface occurs through radiative, convective and conductive mechanisms. The relative contributions depend on a number of factors, including the pool diameter (D). In medium and large-scale pool fires, radiative heat transfer is the dominant mechanism of heat feedback to the fuel surface. In smaller fires, convection and conduction are thought to be important heat feedback mechanisms [5]. Losses to the burner are relatively small for medium scale pool fires [6] and it is reasonable to assume that $\dot{Q}_b$ in Eq. 1 can be neglected. Dividing Eq. 1 by $\dot{Q}$:

$$\chi_a = \chi_r + \chi_c + \chi_s \tag{3}$$

where the fraction of energy from the fire that is radiated to the surroundings (but not back to the fuel surface) is denoted here as the radiative fraction (χ_r):

$$\chi_r = \dot{Q}_r / \dot{Q} \tag{4}$$

The term χ_r represents the integrated radiative flux emitted by the fire in all directions except to the fuel surface, normalized by the fire heat release rate. The fraction of energy from the fire that is convected by the buoyant plume is the convective fraction, χ_c:

$$\chi_c = \dot{Q}_c / \dot{Q} \tag{5}$$

The fraction of energy transported from the fire to the fuel surface is the heat feedback fraction (χ_s):

$$\chi_s = \dot{Q}_s / \dot{Q} \tag{6}$$

The values of the fractional enthalpy terms (χ_r, χ_c, χ_s) vary from fire to fire and are dependent on fuel type, burner diameter, and fire size.

The fractional heat feedback to the fuel surface (χ_s) represents the total heat feedback via radiation, convection and conduction, which can be considered independently. For medium pool diameters, the total heat feedback to the fuel surface ($\dot{Q}_s$) is due to the radiative ($\dot{Q}_{sr}$) and convective ($\dot{Q}_{sc}$) heat feedback incident on the fuel surface:

$$\dot{Q}_s = \dot{Q}_{sr} + \dot{Q}_{sc} \tag{7}$$

Normalizing this expression by the total heat release rate ($\dot{Q}$), the value of χ_s can be broken into its radiative (χ_{sr}) and convective (χ_{sc}) components:

$$\chi_s = \chi_{sr} + \chi_{sc} \tag{8}$$

where the values of χ_{sc} and χ_{sr} in Eq. 8 are normalized by the total fire heat release rate ($\dot{Q}$):

$$\chi_{sc} = \dot{Q}_{sc}/\dot{Q} \text{ and } \chi_{sr} = \dot{Q}_{sr}/\dot{Q} \tag{9}$$

The term χ_{sr} represents the integrated radiative flux emitted by the fire towards the fuel surface, normalized by the fire heat release rate. Khan and Tewarson [7] write Eq. 3 as:

$$\chi_a = \chi_{con} + \chi_{rad} \quad (10)$$

where the combustion efficiency (χ_a) of the heat release rate is broken only into its convective and radiative components. Considering radiative emission from the fire, χ_{rad} can be defined in terms of the total radiative heat transfer to the surroundings and onto the fuel surface such that:

$$\chi_{rad} = \chi_r + \chi_{sr} \quad (11)$$

Determination of the radiative and convective components of heat feedback to the fuel surface ($\dot{Q}_{sr}$ and $\dot{Q}_{sc}$) is challenging. One previous study on methanol estimated the value of the radiative heat flux to the pool everywhere on the surface as approximately equal to the flux measured just outside the burner [8]. Hu et al. used sensors to measure radiative feedback to the fuel surface in small and medium-scale ethanol and heptane pool fires with cross-flow [9]. Yumoto used dual Gardon gauges with different emissivities to measure the heat feedback in medium and large-scale pool fires burning hexane and gasoline [10]. Corlett and Fu estimated the radiative heat transfer on the surface of small and medium-scale methanol and acetone pool fires using a small insulated well filled with fuel [11]. Ref. [6] measured the distribution of incident radiative heat flux across the pool surface in 0.3 m diameter methanol, heptane and toluene pool fires with a nitrogen-purged narrow-view angle gauge. Ring pool mass burning rate measurements provided local total heat flux estimates, allowing determination of (χ_{sr}/χ_s) [6]. A Froude modeling study on gaseous pool fires provided a method to calculate $\dot{Q}_{sc}$ [12] (see discussion below).

The idealized value of χ_s (Eq. 8) is denoted as χ_s^o and is equal to the ratio of the heat per unit time needed to vaporize the liquid fuel ($\dot{Q}_s^o$) to the idealized heat release rate ($\dot{Q}$). The ratio of these parameters is of interest:

$$\chi_s^o = \dot{Q}_s^o / \dot{Q} \quad (12)$$

An energy balance about the liquid fuel pool shows that for a steadily burning fire, the total heat feedback ($\dot{Q}_s$) is equal to the amount of energy required to heat and vaporize the fuel plus other heat transfer terms ($\dot{Q}_{HT}$), including heat transfer to the metal burner walls, re-radiation by the pool surface to the surroundings, reflection of a portion of the incident radiation incident on the pool surface (a function of angle of incidence and the refractive index of the fuel), losses to the burner cooling water, and heat build-up of the liquid pool [6]:

$$\dot{Q}_s^o = \dot{m}\left(\Delta H_L + C_p\,[T_s - T_o]\right) + \dot{Q}_{HT} \quad (13)$$

Dividing both sides of Eq. 13 by $\dot{Q}$ and assuming that the correction term ($\dot{Q}_{HT}$) is relatively small in steady state [6], the value of χ_s^o can be related to the fuel thermochemistry:

$$\chi_s^o = \left(\Delta H_L + C_p\,[T_s - T_o]\right)/\Delta H_c \quad (14)$$

where ΔH_L is the heat of vaporization of the liquid fuel at room temperature, C_p is the average liquid fuel heat capacity between T_s, the temperature of the fuel surface taken as the boiling temperature, and T_o, the initial fuel temperature. The thermochemical properties of the three liquid fuels considered here are characterized by several differences. Table 1 shows the chemical formula, liquid density (ρ), the molecular weight (MW), boiling temperature (T_b), heat of combustion (ΔH_C), heat of vaporization (ΔH_L), and χ_s^o, for the three fuels considered here [13]. All three fuels are oxygenated with boiling points below

that of water. Differences in the values of ΔH_C and ΔH_L are as large as a factor of two among the three fuels, whereas the values of χ_s^o differ by a factor of 3 (with T_s taken as T_b). Thus, a larger fractional amount of the fire's heat release is required to maintain a steady methanol fire as compared to a steady acetone or ethanol fire. The idealized feedback fraction, χ_s^o, is the reciprocal of the diffusive transfer number cited in the literature and influences the fuel mass burning flux [14, 15].

Table 1. Thermochemical properties of methanol, ethanol, and acetone [13].*

Fuel	Chemical Formula	ρ (kg/m^3)	MW (g/mol)	T_b (°C)	ΔH_C (kJ/kg)	ΔH_L (kJ/kg)	χ_s^o
Methanol	CH_3OH	794	32.0	64.7	19.9	1.176	0.059
Ethanol	C_2H_5OH	790	46.1	78.3	26.8	0.930	0.035
Acetone	$(CH_3)_2CO$	792	58.1	56.3	28.6	0.541	0.019
* all parameters in the table are expressed at 20 °C (except T_b, the boiling point). The initial temperature of the fuel was 20 °C in the experiments conducted here, which was ensured by controlling the water cooling temperature on the burner bottom.							

Table 2 lists local and global measurements characterizing the structure of the 0.30 m diameter methanol, ethanol, and acetone pool fires from this and several previous investigations. The measurements reported here complement the previously reported data for these fires and helps build a more complete picture of the energetics, structure and dynamics of medium-scale pool fires. The accumulated information provides a basis for understanding the structure of these fires and makes them interesting candidates for fire model evaluation. These three fires are particularly useful as a testbed for radiation sub-models since blackbody radiation from soot is relatively more or less important depending on the fuel type.

Table 2. List of (previous and current) measurements in well-ventilated, round, steady, 0.30 m diameter pool fires burning in a quiescent environment.

Parameter (units)	References		
	Methanol	Ethanol	Acetone
Mean flame height (m)	16	-	17
Pulsation frequency (Hz)	18	-	19
Radiative fraction (kW/m^2)	8, 16, 20 this study	16, 20, this study	17, 20, this study
Mass loss rate (g/s)	6, 8, 11, 16, 18, 21, this study	11, 20, this study	11, 19, 20, this study
Heat Release Rate (kW)	this study	this study	this study
Radiative flux distribution on fuel surface (kW/m^2)	6	-	-
Total heat flux distribution on fuel surface (kW/m^2)	this study	this study	this study
Radiative flux to surroundings (kW/m^2)	8, 16, this study	this study	this study
Vertical temperature distribution in the fuel (°C)	6	-	-
Gas species volume fraction (mol/mol)	21	-	-
Local Gas Phase Temperature (°C)	18, 21	-	-
Local Gas Phase Velocity (m/s)	18	-	-

This study presents measurements characterizing the energy balance in medium-sized pool fires burning methanol, ethanol, and acetone. The measurements include the time-averaged mass burning and heat release rates as well as the time-averaged local total heat flux onto the pool surface and to the

surroundings. This paper is divided into several parts. In Section 2, the experimental method and apparatus are described. The results are discussed in Section 3 and summarized in Section 4.

2. EXPERIMENTAL METHOD AND APPARATUS

Methanol, ethanol, and acetone pool fires were burned in a quiescent environment within which the radiative emission, total heat feedback to the fuel surface, total heat release rate, sensible enthalpy in the plume, and mass burning rate were measured. Steady-state burning conditions were established before measurements were initiated, which required a warm-up period of 10 min of free burning. The experimental apparatus and method have been previously described in Refs. [6, 16].

2.1 Pool Burner

A circular stainless-steel pan with an inner diameter (D) of 0.301 m, a depth of 0.15 m, and a wall thickness of 0.0013 m was used to hold the liquid fuel. A photograph of the burner is presented in Figure 2. The bottom of the burner had a water-cooled section with thermocouples monitoring the water temperature. The water flow rate was about 1 L/min, ensuring that the bottom of the burner was maintained at a near constant temperature (20 °C ± 2 °C). The burner was mounted on 7.7 cm "legs" such that the top of the burner (its rim) was 0.27 m above the floor. A fuel overflow section included for safety was positioned at 10 cm below the burner rim and extended 2.5 cm in the radial direction beyond the fuel reservoir outer wall. The fuel level was set 10 mm below the top of the burner to match the conditions used in Ref. [18] (see Table 2). Since back diffusion of gas phase water vapor slowly accumulates in the fuel pool [11], fresh fuel was used between experiments.

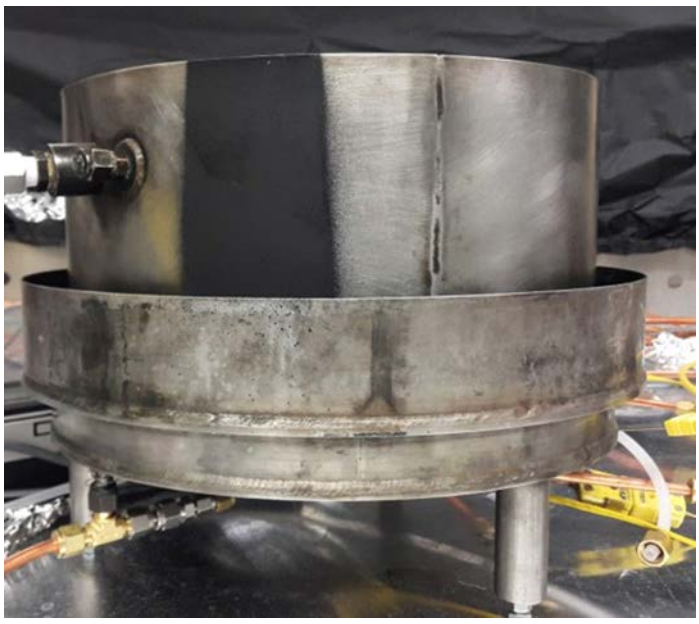

Figure 1. The 0.30 m diameter, water-cooled, stainless-steel, burner with fuel overflow section.

2.2 Exhaust Hood and Compartment

The burner was placed in a compartment with dimensions as indicated in Figure 2. The walls of the compartment (2.5 m by 2.5 m) were formed by a double layer wire mesh screen (6 mesh/cm with 83 % porosity), which created a porous barrier that reduced the influence of room currents on the flow field. The bottom of the exhaust hood (1.8 m by 1.8 m) was positioned 1.9 m above the floor, whereas the exhaust inlet (1.5 m by 1.5 m) was positioned about 2.6 m above the floor. The exhaust flow was maintained at 0.5 kg/s as measured by a system of bidirectional probes and averaging Pitot tubes, which was part of the calorimetry system (described below). The variance of this measurement was less than ± 1 % and the combined expanded uncertainty was estimated as ± 16 %.[*]

2.3 Global Measurements

A number of global fire measurements were made including the mass burning rate and the heat release rate. Unless otherwise mentioned, all measurements were acquired and recorded with a data acquisition system at a rate of 2 Hz.

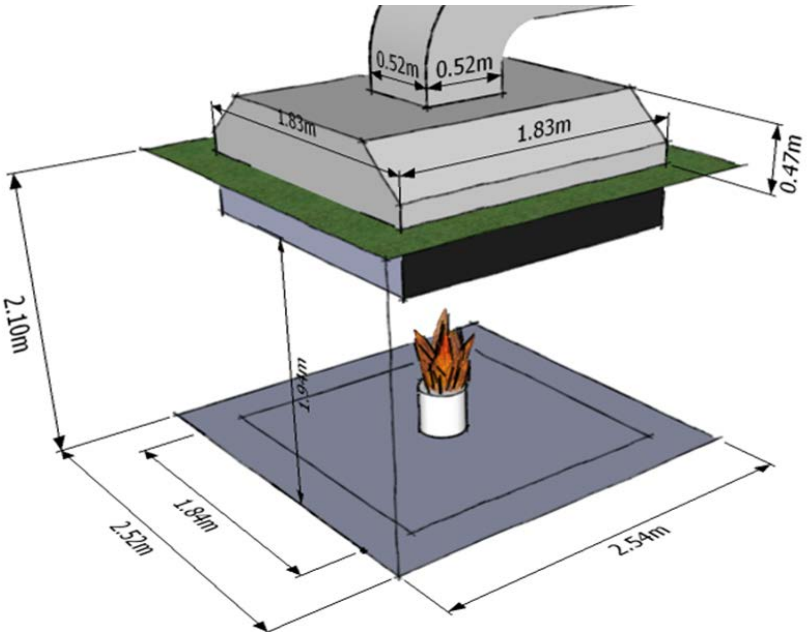

Figure 2. Perspective drawing of the fire compartment and exhaust section. A double wire mesh screen (not shown) formed a porous barrier that reduced the influence of room currents on the flow field.

2.3.1 Mass Burning Rate

Fuel to the burner was gravity fed from a reservoir on a load cell monitored by a data acquisition system. The fuel level was verified throughout the experiment by visually observing the tiny tip of a sharpened (2 mm diameter) pointer that formed a barely discernable bulge on the fuel surface. The level of the fuel

[*] unless otherwise noted, the uncertainty in this paper is expressed as the combined uncertainty with a coverage factor of two, representing a 95 % confidence interval.

was maintained 10 mm below the burner rim by regulating the fuel supply from the reservoir to the burner, using either a thermocouple located just above the pool surface to regulate a solenoid valve in the fuel feed line or by manually adjusting a valve to control the rate of fuel flow. The expanded uncertainty in the fuel level was estimated as 1 mm. The load cell was calibrated with weights of standard mass. Steady burning was typically measured for more than 2000 s. All experiments were repeated at least once.

2.3.2 Heat Release Rate and Convective Enthalpy in the Duct

The convected enthalpy ($\dot{Q}_c$) in the plume was determined from the heat carried by the combustion products through the exhaust duct:

$$\dot{Q}_c = \rho\, V_a\, A\, C_P\, \Delta T \tag{15}$$

where ρ is the mean gas density, V_a is the mean velocity of the exhaust, A is the duct cross-sectional area, C_p is the heat capacity of the exhaust gases, and ΔT is the difference between the ambient temperature and the averaged measured temperature in the duct. The heat capacity and density of the exhaust flow were computed as a function of temperature using the ideal gas law. The gas was composed mainly of air (with only highly dilute amounts of combustion products such as CO_2 and H_2O at values of less than a few percent by volume). With mass conserved in the duct, mass flow measurements were made using two averaging pitot tubes and associated thermocouples oriented horizontally across the exhaust duct at a location approximately 5 m downstream from the exhaust duct entrance. A second measurement station about 6 m downstream from the duct was used to confirm the averaging pitot tube results. The second station consisted of three individual pitot tubes and thermocouples positioned at three vertical locations in the center of the exhaust duct. Each of the pitot tubes were connected to calibrated differential pressure transducers. A third measurement station with thermocouples located about 1 m downstream from the duct entrance provided a way to correct the enthalpy flow in the duct for heat losses to the duct. Measurement of the average temperature difference of the flow at these measurement stations allowed calculation of the heat lost to the duct, enabling correction to the convective enthalpy. The instantaneous temperature and velocity duct measurements were sampled for several mins at a rate of 2 Hz to determine the transient exhaust duct flow.

The total heat release rate was determined from gas sampling in conjunction with the above-mentioned temperature and velocity measurements. Gas samples were extracted from the duct and pulled through a non-dispersive infrared analyzer for determination of the CO and CO_2 volume fractions on a dry basis. A correction based on stoichiometry was applied to convert the measurements to a wet basis. The CO volume fractions were negligible and the total heat release rate ($\dot{Q}_a$) was determined considering the fuel stoichiometry in terms of carbon dioxide production calorimetry:

$$\dot{Q}_a = H_c \frac{\lambda_{fuel}}{\lambda_{CO_2}} \frac{MW_{fuel}}{MW_e} X_{CO_2} \dot{m}_e \tag{16}$$

where λ_i is the stoichiometric coefficient of species i, X_{CO_2} is the volume fraction of carbon dioxide in the exhaust stream, $\dot{m}_e$ is the mass flow rate of the exhaust, and MW_{fuel} *and* MW_e are the molecular weight of the gaseous fuel and the exhaust flow, respectively. Since the gases sampled from the duct were dried

before measurement in the gas analyzers, the gas concentration measurements were corrected for water. The relationship between the wet and dry CO_2 volume fractions is given by Ref. [22]:

$$X_{CO_2,wet} = \frac{X_{CO_2 dry}}{1+\frac{y}{2x} X_{CO_2 dry}} \tag{17}$$

where x and y denote the number of carbon and hydrogen atoms, respectively, in the original fuel molecule (see Table 1).

2.4 Local Measurements

2.4.1 Total Heat Flux towards the Pool Surface

The total local heat flux incident on the pool surface controls the fuel mass burning rate (see Eqs. 13 and 14). The time-averaged local heat flux in the downward direction onto the fuel surface (-z direction in Figure 3) was measured with a calibrated, water-cooled, Gardon-type total heat flux gauge positioned just above the fuel surface. The gauge was a specially designed 1.25 cm diameter (1.0 cm depth) circular gauge with the sensing portion of the gauge positioned 3 mm ± 1 mm above the burner rim. The gauge was translated above the surface of the pool such that the total heat flux was determined as a function of distance from the pool center. The signal output and the water cooling in/out lines (3 mm outer diameter) were embedded within a straight 9 mm (3/8 in) diameter metal tube connected to the side of the gauge.

The water-cooling pump system provided a controlled source of heated water near the fuel boiling point (see Table 1) to the gauge, which prevented fuel condensation on the gauge surface. Observation of the gauge surface confirmed its status as dry or wet. Positioning the gauge at lower positions in the pool intermittently led to spurious results, possibly associated with liquid fuel boiling around the bottom of the hot gauge, causing liquid fuel blockage on the sensor surface. Thermocouples on the cooling lines entering and exiting the gauge provided a measure of the gauge temperature, which remained nearly constant during the experiment. On average, the variance in the heat flux measurement ranged from 8 % to 30 %, depending on the fuel type and the location of the gauge in the fire.

Assuming symmetry and integrating the measured total local time-averaged heat flux measured in the downward direction towards the fuel surface, just above the burner rim, $\dot{q}_s''(r, z = 0)$, provided an estimate of the total heat flux onto the pool surface ($\dot{Q}_s$):

$$\dot{Q}_s = 2\pi \int_0^{R_b} \dot{q}_s''(r)\, r\, dr \tag{18}$$

where R_b is the pool radius (0.15 m). The total heat transfer to the fuel surface can be broken into radiative and convective components following Eq. 7. Applying stagnant film theory, the convective heat transfer to the fuel surface ($\dot{Q}_{sc}$) can be estimated following Ref. [23]:

$$\dot{Q}_{sc} = A \left(\frac{h}{C_p}\right) [\Delta H_c\, (\chi_a - \chi_r)\, r/\chi_a - C_p(T_s - T_\infty)]\, y/(exp(y) - 1) \tag{19}$$

where A is the pool surface area, y (= $\dot{m}'' C_p/h$) is a blowing factor, $\dot{m}''$ is the mass flux (i.e., the burning rate per unit surface area of the burning pool), r is the stoichiometric fuel/air mass ratio, T_s is the burner

surface temperature, T_∞ is the ambient temperature, and C_p is the heat capacity of air taken here at 750 K, which is representative of a temperature intermediate between the flame temperature and the burner surface temperature. The heat transfer coefficient (h) is taken as 8.5 W/(m^2-K) for pools with "lips" [12]. A description of application of this approach is given in Ref. [23].

2.4.2 Heat Flux to the Surroundings

The local time-averaged radiative heat flux distribution, $\dot{q}''(r,z)$, along a cylindrical control surface surrounding the fire was measured using a set of calibrated water-cooled radiometers and heat flux gauges with a wide angle (150° view angle) coated with high emissivity paint that had a flat spectral response. These measurements complemented measurements of the flux onto the pool surface. A series of water-cooled Schmidt-Boelter type total heat flux transducers were positioned along perpendicular axes aligned with the burner rim to measure the radiative heat flux to the surroundings. During some experiments, water-cooled Schmidt-Boelter type radiometers with windows positioned on translation stages were used to confirm the results using the windowless sensors. Figure 3 shows a schematic diagram of the experimental set-up. The radiative energy distribution was mapped onto a cylindrical control surface surrounding the fire with the base of the cylinder defined by the plane of the fuel surface. The gauges were positioned on a vertical axis located 60 cm from the pool fire's central axis (R_o in Figure 3) with the gauges oriented towards the fire. A row of gauges was also positioned along a radius on the plane aligned with the burner rim oriented in an upward direction. The radiative flux typically decreased steeply in the radial direction, whereas in the vertical direction, the flux peaked at a vertical location equal to approximately one-half of the characteristic flame height and then decreased above the visible flame tip. The gauges were calibrated using a secondary standard in a well-characterized radiometer facility [24]. The measured signal was recorded at 2 Hz and time-averaged over a minimum of 60 s, representing about 200 cycles of the pulsing fires.

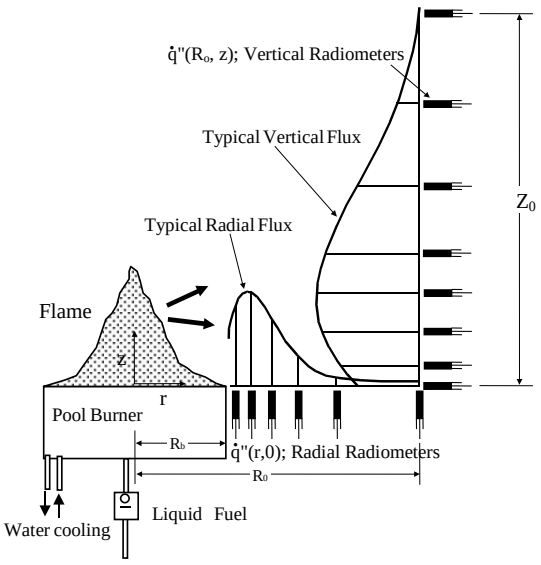

Figure 3. A schematic diagram of the set-up used in the measurement of radiative flux to the surroundings. The total heat flux 3 mm above the fuel surface as a function of radial location in the pool was also measured.

Integrating the measured local radiative heat flux in the r and z directions (see Figure 3) yields $\dot{Q}_r$, considering the flux through a cylindrical control surface about the pool fire:

$$\dot{Q}_r = 2\pi \int_{r=R_b}^{R_o} \dot{q}''(r, z=0)\, r\, dr \;+\; 2\pi\, R_o \int_{z=0}^{Z_o} \dot{q}''(R_o, z)\, dz \tag{20}$$

where Figure 3 delineates the limits of integration. Measurement uncertainty was estimated considering the uncertainties associated with repeat measurements and a propagation of error analysis [25]. Unless otherwise noted, uncertainties are reported as the combined expanded uncertainty with an expansion factor of two, corresponding to a confidence level of approximately 95 %.

3. RESULTS AND DISCUSSION

Figure 4 shows snapshots of the pulsing methanol, ethanol, and acetone pool fires burning in the 0.30 m stainless-steel water-cooled burner. The shape and apparent color of the fires differed among the three fuel types. A series of repeated cycles were observed in the fires, where the curved flame sheets were anchored at the burner rim and connected to the base of the fire, rolling towards the fire centerline and necking-in to form a narrow and long visible fire plume. The methanol fire was entirely blue, whereas the ethanol and acetone fires were luminous. The necking region was relatively narrow for the methanol fire compared to the ethanol and acetone fires. The methanol fire appeared to be weakly turbulent whereas the ethanol, and even more so, the acetone fire, was characterized by turbulent structures. The observed dynamic fire shapes were consistent with the description given by Weckman and Sobiesiak for a medium-scale acetone pool fire [19] and with the analysis given by Baum and McCaffrey [26]. The methanol and ethanol flames appeared to attach to the inside of the burner rim wall and flow near the pool surface towards the pool center, whereas the acetone flames appeared to attach at a higher location on the burner rim with the flams lifter off the pool surface at an angle as seen in the images shown in Figure 4. The time-averaged flame height of the methanol fire was the smallest, followed by ethanol and then acetone.

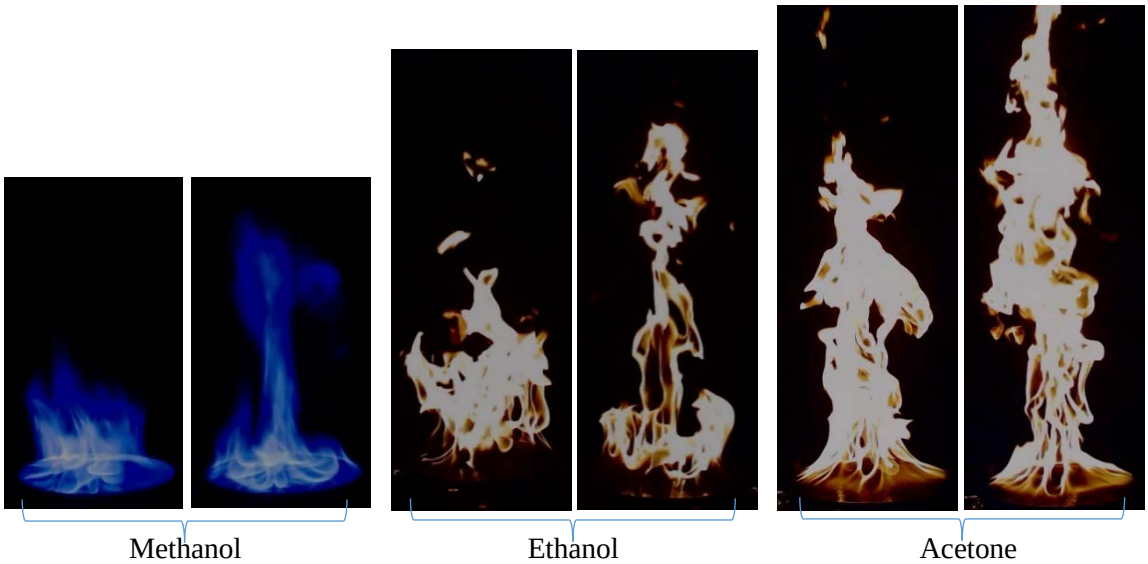

Figure 4. Typical instantaneous digital images of the tallest and shortest flame lengths during a cycle of the pulsing 0.30 m diameter methanol (left), ethanol (center) and acetone (right) pool fires.

3.1 Heat Release and Mass Burning Rates

The measured time-averaged mass burning fluxes are listed in Table 3 for the methanol, ethanol, and acetone pool fires. Also listed are the calculated heat flux to the fuel surface needed to evaporate the mass burning flux ($\dot{Q}_s^{o"}$) and the idealized heat release rate ($\dot{Q}$) from measurement of the time-averaged mass loss, using Eqs. 13 and 2, respectively.

Table 3. Measured mass burning flux in the 0.30 m pool fires, the heat required to vaporize the fuel, and the idealized heat release rate.

Fuel	$\dot{m}"$ (g/m^2-s)	$\dot{Q}_s^o$ * (kW)	$\dot{Q}$ ** (kW)
Methanol	13.5 ± 9 %	1.13 ± 9 %	19.2 ± 9 %
Ethanol	16.2 ± 11 %	1.07 ± 11 %	31.0 ± 11 %
Acetone	18.7 ± 11 %	0.72 ± 11 %	38.1 ± 11 %
* see Eq. 13 ** see Eq. 2			

Table 4 shows the values of previous mass burning flux measurements for 0.30 m diameter pool fires with constant and varying lip height conditions. The values reported here (Table 3 and Table 4 are generally in agreement with previous measurements within experimental uncertainty.

Table 4. Previous results reported for the mass burning flux in 0.30 m pool fires.

Fuel	$\dot{m}"$ (g/m^2-s)	constant lip height	lip height (mm)
Methanol	12.7 [16]	yes	10
	15.2 [18]	yes	1
	12.7 [6]	no	-
	13 [20]	yes	10
	12.5 [11]	yes	1
Ethanol	15 [20]	yes	10
	13.8 [11]	yes	1
Acetone	15.0 [19]	yes	10
	18.3 [11]	yes	1
	18 [20]	yes	10

Table 5 compares the values of $\dot{Q}$ (taken from Table 3) with the calorimetric heat release rate ($\dot{Q}_a$) and convective enthalpy ($\dot{Q}_c$) measured in the exhaust duct. The correction for $\dot{Q}_c$ for heat loss through the duct walls was on-average about 2 % of the measured enthalpy flow for the three fires. A comparison of the fractional enthalpy convected ($\chi_c = \dot{Q}_c/\dot{Q}$) (from Eq. 5) shows that a majority of the fire's energy is convected for all three fires with their values within 15% of each other. A comparison of $\dot{Q}_c$ and $\dot{Q}_a$ shows that about 70 % to 80 % of the fire's energy was convected with the largest value occurring in the methanol fire.

Table 5. Heat release rate, convected enthalpy, and fractional convective enthalpy in the exhaust of the 0.30 m pool fires.

Fuel	$\dot{Q}$ (kW)	$\dot{Q}_a$ * (kW)	$\dot{Q}_c$ ** (kW)	$\chi_c\ (=\dot{Q}_c/\dot{Q})$ ***
Methanol	19.2 ± 9 %	17.3 ± 18 %	14.4 ± 14 %	0.75 ± 17 %
Ethanol	31.0 ± 11 %	28.5 ± 18 %	21.1 ± 14 %	0.68 ± 18 %
Acetone	38.1 ± 11 %	37.8 ± 18 %	26.7 ± 14 %	0.70 ± 18 %
* see Eq. 16 ** see Eq. 15 *** see Eq. 5				

Figure 5 presents the data in Table 5 in which the idealized heat release rate ($\dot{Q}$) based on the measured mass burning flux is presented as a function of $\dot{Q}_a$, the measured heat release rate for each of the fuels. The results showed that $\dot{Q}$ and $\dot{Q}_a$ differ by about 7 % on-average, suggesting that the combustion efficiency was close to unity for these pool fires. The measurement of negligible amounts of CO in the exhaust stream was consistent with this result.

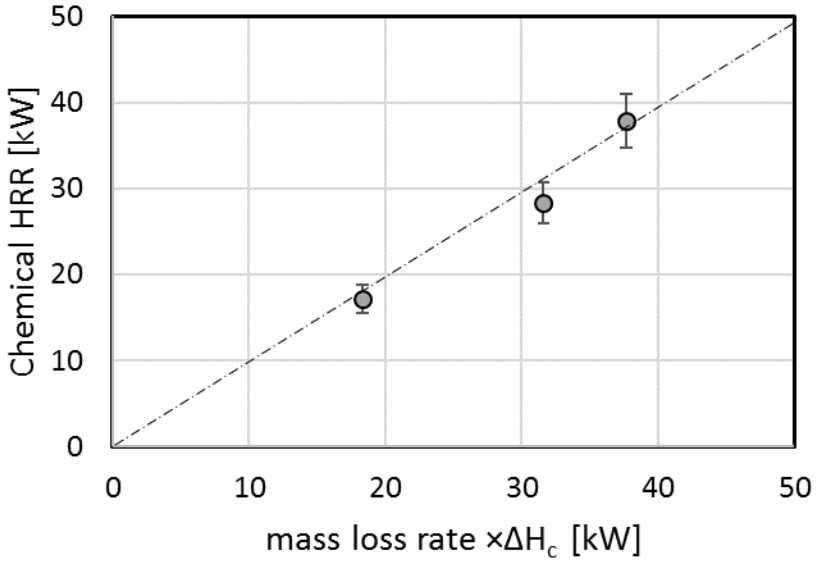

Figure 5. The measured heat release rate ($\dot{Q}_a$) determined by calorimetry compared to the idealized heat release rate determined from the mass loss measurement ($\dot{Q}$).

3.1 Heat Feedback to the Pool

Figure 6 shows the transient local total heat flux 3 mm above the burner rim as a function of time in the methanol pool fire as the gauge was moved across the pool surface during the experiment. The dotted lines indicate the radial location of the gauge. Measurements were made for about 60 s at each location, which represented about 200 cycles of these pulsing pool fires. The measurements displayed some variation during the period when the gauge was stationary. The reasons for this were unclear but could have been related to changes in the height of the fuel surface or changes in flame tilt as a result of room

air currents (e.g., a lab door opening). Repeat measurements helped provide confidence in the reported results. In Figure 6, the measurement and its variance appeared to be particularly large towards the pool center (R < 12 cm).

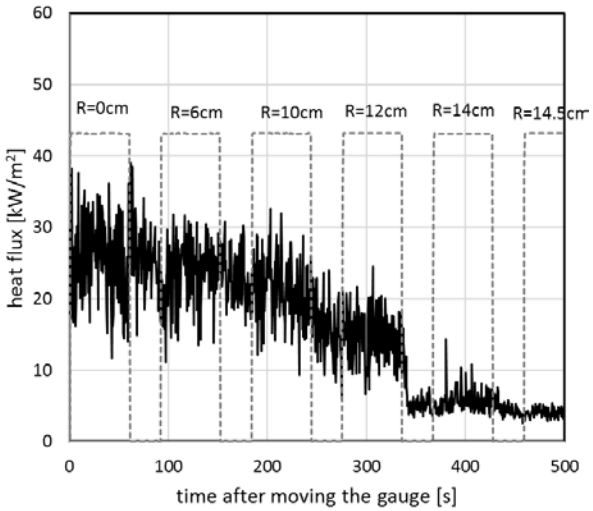

Figure 6. The transient local total heat flux 3 mm above the burner rim as a function of time for the methanol pool fire. The numbers above the dotted lines indicate the radial location of the gauge during the experiment. The period between the dotted lines represents times when the gauge was moved to the next measurement location. The position R=0 refers to the pool center.

Figure 7 shows the time-averaged local total heat flux 3 mm above the burner rim as a function of distance from the pool center for the methanol pool fire based on three independent experiments. The average heat flux was about constant near the pool center (R < 6 cm), and then decreased with distance towards the pool edge.

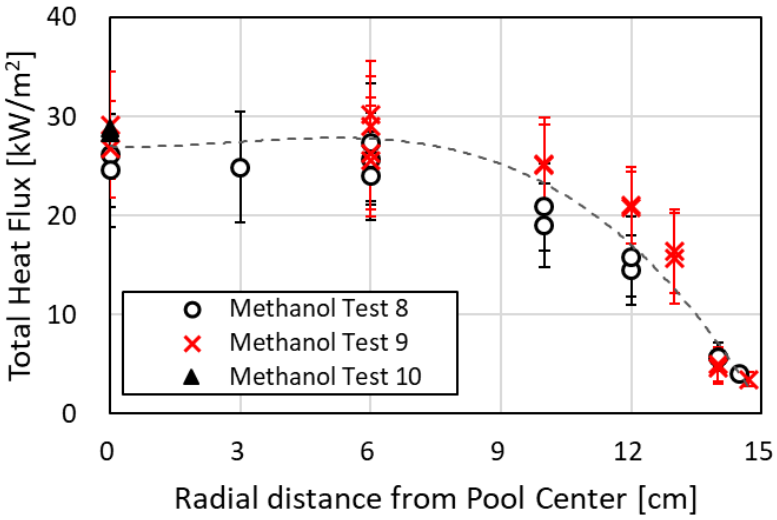

Figure 7. The time-averaged total local heat flux measured in the downward direction as a function of radial distance from the pool center 3 mm above the burner rim in the 0.30 m diameter methanol pool fire for three experiments (labeled Tests 8, 9, and 10). The uncertainty bars represent the standard deviation of the measurement.

The uncertainty bars in Figure 7 represent the standard deviation of the variance associated with each individual measurement. Integrating the flux over the fuel surface yields 1.6 kW on-average, which is a factor of 1.4 larger than the value of $\dot{Q}_s^o$ (=1.13 kW) shown in Table 3. The difference in these values may be due to (1) heat losses to the burner and (2) that the measurements were not made exactly at the fuel surface, but at a location 3 mm above the rim (13 mm above the fuel surface) due to experimental limitations. The actual total heat flux at the pool surface ought to be lower than the values reported in Figure 7 as convective and radiative heat transfer processes are sensitive to position due to fuel vapor absorption and differences in the flow field which affects local convective heat transfer.

A measure of this effect is presented in Figure 8, where the total heat flux at the pool center is shown as a function of distance above the burner rim. The measurements showed that the heat flux first increased with distance above the pool and then decreased. Lowering the gauge further towards the fuel surface led to wetting of the gauge surface, resulting in diminished values of the measured heat flux (see the figure). Extrapolating the results suggests that the difference between the total heat flux measured 3 mm above the burner rim and the flux at the fuel surface was approximately 15 % for the 0.30 m diameter methanol fire at the pool center. Measurements by Yilmaz [27] above the centerline of a specially designed 0.30 methanol pool fire using a Fourier Transfer Infrared Spectrometer indicates that radiation blockage by methanol and other participating species near the fuel surface was less than 1 % over the 13 mm distance between the gauge and the fuel surface. Differences were more likely due to details associated with how the time-varying flow field near the fuel surface impacted convective heat transfer.

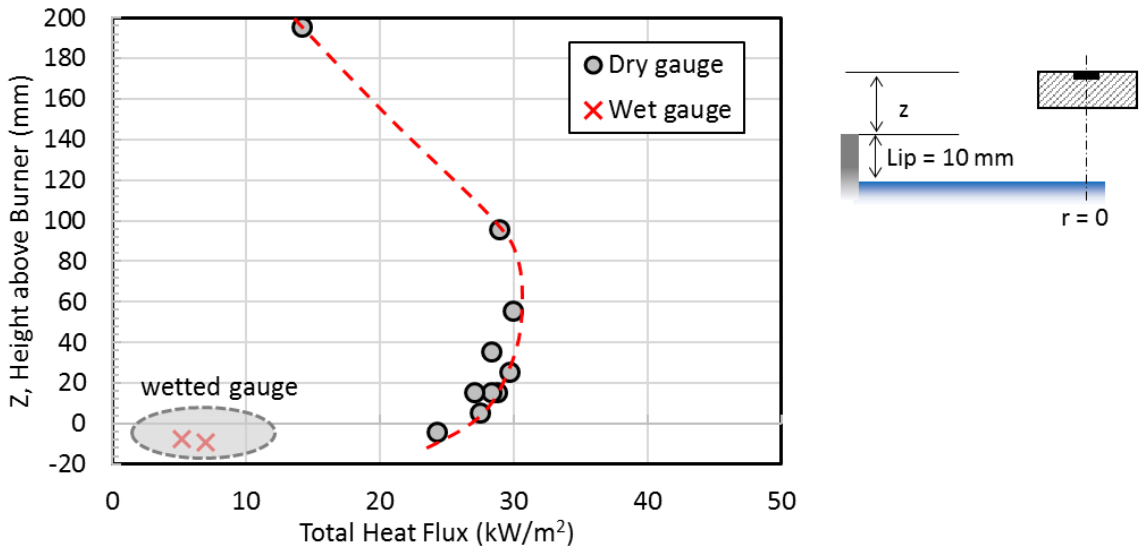

Figure 8. The time-averaged total local heat flux at the pool center as a function of distance (Z) above the burner in the 0.30 m diameter methanol fire with the lip height fixed at 10 mm. Observations of the gauge surface as wet or dry are noted. A schematic of the configuration is presented to the right of the graph.

Measurements analogous to Figure 7 are shown for the ethanol and acetone fires in Figure 9 and Figure 10, respectively, in which the time-averaged total local heat flux measured in the downward direction is shown as a function of radial distance from the pool center with the gauge located 3 mm above the burner rim and the lip height maintained at 10 mm. The uncertainty bars represent the variance of each measurement. A best fit curve is also shown. For the ethanol fire, integrating the incident total heat flux

over the fuel surface yields 1.56 kW, which is 22 % larger than the idealized value required to evaporate the fuel (see Table 3).

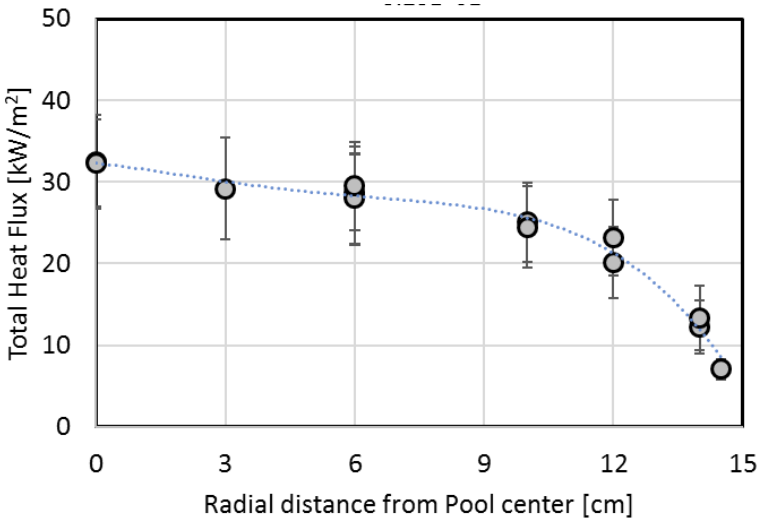

Figure 9. The time-averaged total local heat flux measured in the downward direction as a function of radial distance from the pool center 3 mm above the burner rim in the 0.30 m diameter ethanol pool fire. The uncertainty bars represent the standard deviation of the measurement.

The heat flux profile for the acetone fire, shown in Figure 10, was qualitatively different than that of the other fuels. Several repeat measurements were conducted. The total heat flux was relatively flat Near the burner edge, the measurement variance was relatively large compared to the pool center. And the measurement variance near the edge of the burner was larger in the acetone fire than in the methanol or ethanol fires (see Figures 6, 7 and 9). This may have been due to the way the acetone fire was anchored to the burner rim (see Figure 4 and its discussion). The anchoring region of a pool fire is geometrically and temporally complex, composed of nodes and ventral segments that are intermittent [18, 28]. For the acetone fire, the burning rate was significantly larger than the methanol and ethanol fires, the flames were taller, and the anchoring position of its flames were higher on the burner rim. Measurement of the heat flux was particularly sensitive to small changes in the relative position of the sensor to the flames.

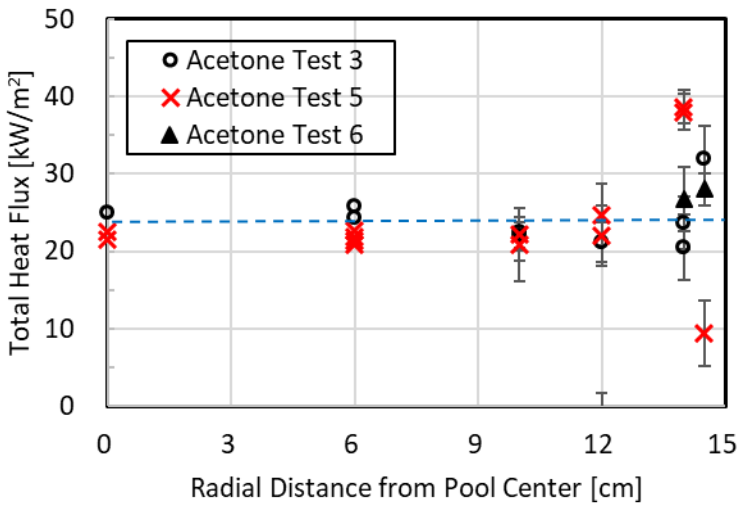

Figure 10. The time-averaged total local heat flux measured in the downward direction as a function of radial distance from the pool center and 3 mm above the burner rim in the 0.30 m diameter acetone pool fire. The uncertainty bars represent the standard deviation of the measurement.

Table 6 shows the results of calculations to determine the total, or integrated value, of the measured time-averaged total heat flux to the fuel surface ($\dot{Q}_s$). Best fit polynomial curves from the data presented in Figure 7, Figure 9, and Figure 10 were used to determine the average flux as a function of location. Then, Eq. 18 was used to determine the total integrated heat flux. Table 6 also lists the heat feedback fraction (χ_s) based on $\dot{m}$" (from Table 3) and Equation 6, the calculated values of $\dot{Q}_{sc}$, χ_{sc}, χ_{sr}, and the ratio, χ_{sr}/χ_s, (see Eqs. 7 and 9). The table shows that the values of χ_s are significantly larger than the idealized values for χ_s^o listed in Table 1, presumably due to heat losses.

Table 6. Integrated value of the total heat flux ($\dot{Q}_s$) measured just above the pool surface, the calculated convective heat feedback ($\dot{Q}_{sc}$) at the pool surface, and the associated fractional total heat feedback enthalpy (χ_s), its convective (χ_{sc}) and radiative (χ_{sr}) components, and the fractional radiative heat feedback (χ_{sr}/χ_s) in 0.30 m pool fires.

Fuel	$\dot{Q}_s$ * (kW)	$\dot{Q}_{sc}$ (kW)	χ_s**	χ_{sc} ***	χ_{sr} ***	χ_{sr}/χ_s
Methanol	1.6 ± 24 %	0.52 ± 17 %	0.082 ± 24 %	0.027± 41 %	0.055 ± 21 %	0.67 ± 21 %
Ethanol	1.6 ± 24 %	0.25 ± 21 %	0.050 ± 24 %	0.008± 30 %	0.042 ± 16 %	0.84 ± 29 %
Acetone	1.7 ± 24 %	0.20 ± 26 %	0.043 ± 24 %	0.005± 29 %	0.038 ± 15%	0.88 ± 29 %

* see Eq. 18
** see Eq. 6
*** see Eq. 9

Previous calculations have highlighted the relative importance of convective heat transfer to the fuel surface for pool fires, particularly when blowing (i.e., the burning rate) is relatively small [23]. The values of the ratio, χ_{sr}/χ_s, presented in Table 6 show that radiation is the dominant heat feedback mechanism in all three fires considered here, although convection also plays a significant role – particularly for methanol. Of the three fires considered here, the methanol pool has the slowest mass

burning rate and the largest estimated values of $\dot{Q}_{sc}$ and χ_{sc}. For the methanol fire, about 67 % of the energy transferred to the pool surface from the fire was attributed to radiation (see χ_{sr}/χ_s in Table 6), which is within experimental uncertainty of the value (= 55 %) reported in Ref. [6] for methanol pool fire experiments conducted using the same burner but with a slightly different lip height (5 mm in Ref. [6] as compared to 10 mm in this study).

3.3 Local Heat Flux Distribution

Figure 11 compares the local time-averaged radiative heat flux measured in the downward (-z direction in Figure 3) as a function of radial distance from the pool center outside the methanol, ethanol and acetone pool fires. The values of the total heat flux in the downward direction was highly similar in the ethanol and acetone fires, which were both larger than the methanol fire. Each of the methanol data points are within 10 % of the measurements previously reported by Klassen and Gore using the same burner [8].

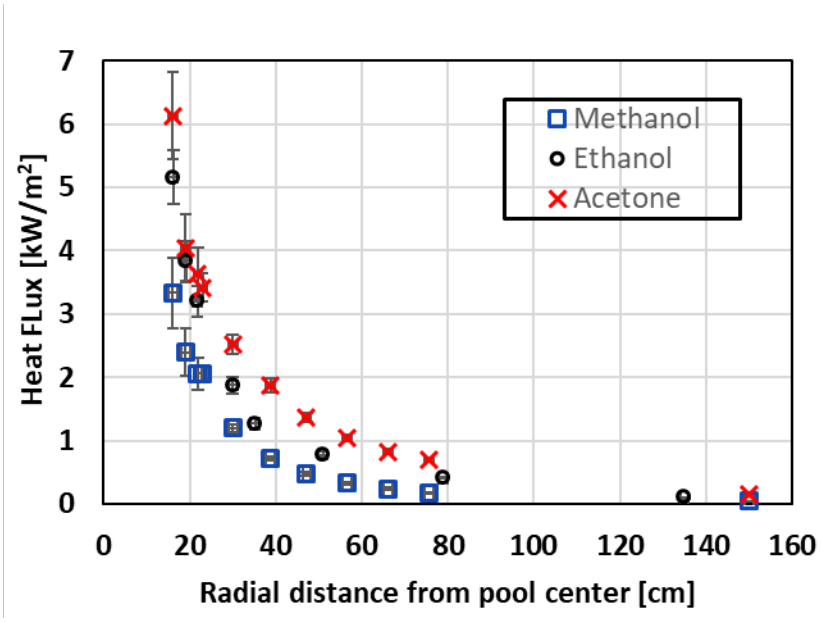

Figure 11. The time-averaged local radiative heat flux measured in the downward direction as a function of radial distance from the pool center outside the 0.30 m diameter methanol, ethanol and acetone pool fires. The uncertainty bars represent the standard deviation associated with measurement variance.

Figure 12 compares the local time-averaged radiative heat flux measured in the horizontal direction away from the fire as a function of vertical distance above the plane defined by the burner rim for the methanol, ethanol and acetone pool fires at a distance of 0.60 m (Ro in Fig. 1) from the burner center. The largest value of the heat flux was observed in the acetone fire followed by the ethanol and methanol fires.

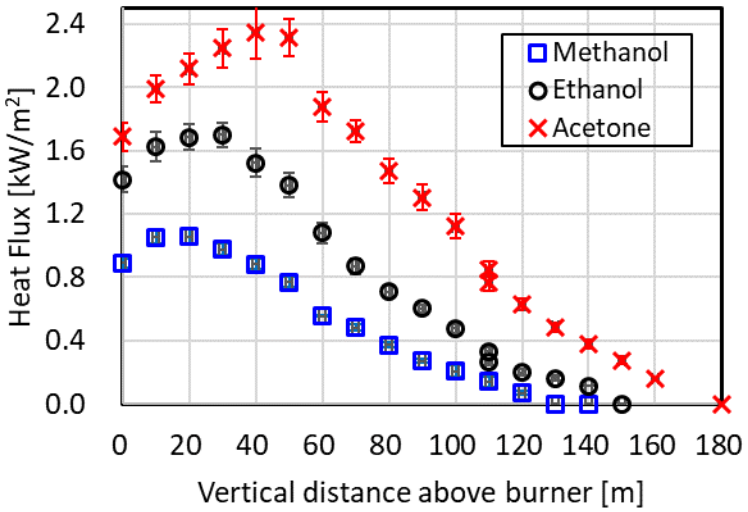

Figure 12. The local time-averaged radiative heat flux measured in the horizontal (radial) direction away from the fire as a function of vertical distance above the plane defined by the burner rim for the methanol, ethanol and acetone pool fires at 60 cm from the pool center (Ro in Fig. 1). The uncertainty bars represent the standard deviation of the measurement.

Radiation plays an important role in heat transfer in these pool fires. The results shown in Figure 11 and Figure 12 can be used to determine χ_r using Eq. 4, where the total radiative heat transfer through a control surface defined by a cylinder surrounding the fire is considered (following Eq. 20 as illustrated in Figure 2). Table 7 lists χ_r as well as χ_{sr} and χ_{rad} (see Eqs. 4, 9 and 11). Careful radiative emissive power measurements on 0.305 m acetone pool fires reported χ_{rad} values from 0.22 to 0.29, depending on the technique used [17]. Previous studies in 0.30 m pool fires reported χ_r equal to 0.18 ± 10 % [16], 0.17 [6] and 0.22 [20] for methanol, 0.17 ± 10 % [16] for ethanol, and 0.27 [20] for acetone, which are in general agreement with the results reported here within overlapping experimental uncertainties.

The results of the current study listed in Table 7 show that the acetone fire had the largest value of χ_{rad} and the smallest value of χ_{sr}, whereas the methanol fire had the smallest value of χ_{rad} and the largest value of χ_{sr}. This is not unexpected as the methanol fire was with little or no soot (as seen in Figure 4), so its radiative emission was relatively smaller compared to the ethanol and acetone fires.

Table 7. Comparison of radiation terms following Eq. 11

Fuel	χ_{sr}	χ_r	χ_{rad}
Methanol	0.055 ± 21 %	0.18 ± 26 %	0.26 ± 25 %
Ethanol	0.042 ± 16 %	0.21 ± 26 %	0.26 ± 25 %
Acetone	0.040 ± 15 %	0.27 ± 26 %	0.31 ± 25 %

3.4 Enthalpy Balance

Table 8 lists the values of key parameters including the radiative heat emitted by the fire to the surroundings (χ_r), the enthalpy convected by the plume (χ_c), and heat feedback to the fuel surface (χ_s). The values of the parameters contribute to the burning characteristics of a pool fire. The sum of the energy terms provides a check on the energy balance, which shows that the results are on-average within 3 % of unity. The results show that both radiation and convection play significant roles in the pool fires studied here. Radiation was the dominant mechanism of heat feedback to the fuel surface, accounting from about 67 % to 88 % of the heat feedback (see the ratio χ_{sr}/χ_s in Table 6), while enthalpy convected in the plume represented about 68 % to 75 % of the fire's total energy (see χ_c in Table 8), exceeding radiative emission to the surroundings.

Table 8. Enthalpy balance following Eq. 3

Fuel	χ_s *	χ_r**	χ_c ***	Sum
Methanol	0.082 ± 24 %	0.19 ± 26 %	0.75 ± 17 %	1.02 ± 19 %
Ethanol	0.050 ± 24 %	0.21 ± 26 %	0.68 ± 18 %	0.95 ± 20 %
Acetone	0.046 ± 24 %	0.27 ± 26 %	0.70 ± 18 %	1.02 ± 20 %
* see Eq. 6 ** see Eq. 4 *** see Eq. 5 and Table 5				

4. SUMMARY

A series of measurements were conducted to characterize the structure of 0.30 m diameter well-ventilated methanol, ethanol, and acetone pool fires burning in a quiescent environment. Time-averaged global and local parameters were measured. The measurements reported here complement previously published data for these fires, including the mass loss rate, energy balance, radiative flux distribution to the surroundings, and heat flux distribution onto the fuel surface, as noted in Table 2. An enthalpy balance was considered to characterize pool fires burning three fuels. The study can be summarized as follows:

- The results show that both radiation and convection played significant roles in the pool fires studied here.
- Radiation was the dominant heat feedback mechanism to the fuel surface, accounting from about 67 % to 88 % of the heat feedback
- Enthalpy convected in the plume represented about 68 % to 75 % of the fire's total energy, exceeding radiative emission to the surroundings.
- As expected, the value of χ_r was smallest for the non-luminous methanol fire.

The measurements reported here help to build a picture of the global heat transfer processes governing the energetics of steadily burning 0.30 m diameter methanol, ethanol, and acetone pool fires. These results

along with complementary data in the technical literature begin to form the basis for a better understanding of the structure of the medium-scale pool fires investigated here, making them suitable candidates for fire model evaluation studies. Analogous measurements on the effect of fire size on the energetics of pool fires would also be of value.

5. ACKNOWLEDGEMENTS

The authors are grateful to Marco Fernandez of NIST for helping to construct the wire mesh compartment used in the experiments and to Takashi Kashiwagi, Jay Gore, and Howard Baum for helpful discussions.

6. REFERENCES

1. Peacock, R.D., Reneke, P.A., Forney, G.P., CFAST – Consolidated Model of Fire Growth and Smoke Transport (Version 6), NIST Special Publication 1041r1, March 2013. http://dx.doi.org/10.6028/NIST.SP.1041r1v

2. McGrattan, K., McDermott, R., Hostikka, S., Floyd, J., Weinschenk, C., Overholt, K., Fire Dynamics Simulator, National Institute of Standards and Technology, Gaithersburg, MD, NIST Special Publication 1019, Sixth Edition, April 2016. http://dx.doi.org/10.6028/NIST.SP.1019

3. Hu, L., A review of physics and correlations of pool fire behaviour in wind and future challenges, Fire Safety Journal 91, 41–55 (2017). https://doi.org/10.1016/j.firesaf.2017.05.008

4. Joulain, P., Proc. 27th Sym (International) on Comb., The Behavior of Pool Fires, 2691–2706, (1998).

5. Hottel, H.C., Certain Laws Governing Diffusive Burning of Liquids, *Fire Research Abstracts Reviews* 1: 41-53, 1959.

6. Hamins, A., Klassen, M., Gore, J., Fischer, S., and Kashiwagi, T., Heat Feedback to the Fuel Surface in Pool Fires, *Combust. Sci. Tech*., **97**, 37-62 (1993).

7. Khan, M.M. and Tewarson, A., Combustion Characteristics of Materials and Generation of Fire Products, Chapter 36 in the *SFPE Handbook of Fire Protection Engineering* (Fifth Ed.; M. Hurley Ed.), Springer, New York, 1143 – 1232, 2016. DOI 10.1007/978-1-4939-2565-0_36

8. M. Klassen and J.P. Gore, Structure and Radiation Properties of Pool Fires, *NIST Report GCR-94-651*, National Institute of Standards and Technology, Gaithersburg, MD, June 1994.

9. Hu, L., Liu, S., and W. Wu, Flame radiation feedback to fuel surface in medium ethanol and heptane pool fires with cross air flow Comb. & Flame, 160, 295–306 (2013). https://doi.org/10.1016/j.combustflame.2012.10.016

10. Yumoto, T., Heat Transfer from Flame to Fuel Surface in Large Pool Fires, *Combust. Flame*, **17**, 108 (1971).

11. Corlett, R.C., and Fu, T.M., Some Recent Experiments with Pool Fires, *Pyrodynamics*, 1, 253-269 (1966).

12. Orloff, L. and de Ris, J., Froude Modeling of Pool Fires, *Technical Report FMRC OHON3.BU, RC81-BT-9*, Factory Mutual Research Corp., Norwood, MA, October 1983.

13. Design Institute for Physical Properties (DIPPR 801), American Institute of Chemical Engineers (2017). https://dippr.byu.edu

14. Spalding, D.B., Some Fundamentals of Combustion, Batterworth, London, England, 1955.

15. Burgess, D., and Hertzberg, M., *Radiation from Pool Flames* in Afgan, N.H., and Beers, J.M. (Eds.), Heat Transfer in Flames, John Wiley & Sons, New York, Chapter 27, 1974.

16. Hamins, A., Klassen, M., Gore, J., and Kashiwagi, T., Estimate of Flame Radiance via a Single Location Measurement in Liquid Pool Fires, *Combustion and Flame*, 86:223-228 (1991).

17. Hogben, C.D.A, Young, C.N., Weckman, E.J., and Strong, A.B., Radiative Properties of Acetone Pool Fires, *33rd ASME National Heat Transfer Conference*, Albuquerque, NM, August 1999.

18. Weckman, E.J., and Strong, A.B., Experimental investigation of the turbulence structure of medium-scale methanol pool fires, *Combustion and Flame*, 105: 245-66 (1996).

19. Weckman, E.J., and Sobiesiak, A., The Oscillatory Behavior of Medium-Scale Pool Fires, *Proceedings of the Twenty-Second Sym. (Int.) on Combustion*, The Combustion Institute, 1299-1310 (1988). 20. Buch, R., Hamins, A., Konishi, K., Mattingly, D., and Kashiwagi, T., Radiative Emission Fraction of Pool Fires Burning Silicone Fluids, *Combust. Flame*, **108**, 118-126 (1997).

21. Hamins, A., and Lock, A., The Structure of a Moderate-Scale Methanol Pool Fire, National Institute of Standards and Technology, Gaithersburg, MD, NIST Technical Note 1928, Oct. 2016.

22. Bundy, M., Hamins, A., Johnsson, E.L., Kim, S.C., Ko, G.H., Lenhert, D.B., Measurements of Heat and Combustion Products in Reduced-Scale Ventilation-Limited Compartment Fires, NIST Technical Note 1483, National Institute of Standards and Technology, Gaithersburg, MD, July 2007.

23. Hamins, A., Energetics of Small and Moderate-Scale Gaseous Pool Fires, NIST Technical Note 1926, National Institute of Standards and Technology, Gaithersburg, MD, October 2016. https://doi.org/10.6028/NIST.TN.1926

24. Pitts, W.M., Lawson, J.R., and Shields, J.R., NIST/BFRL Calibration System for Heat-Flux Gages, Report of Test FR 4014, National Institute of Standards and Technology, Gaithersburg, MD, August 6, 2001.

25. Taylor, B.N., and Kuyatt, C.E., Guidelines for Evaluating and Expressing the Uncertainty of NIST Measurement Results. NIST Technical Note 1297, National Institute of Standards and Technology, Gaithersburg, MD, 1994.

26. Baum, H. R., and McCaffrey, B. J., Fire Induced Flow Field - Theory and Experiment, *Proceedings of the Second International Symposium on Fire Safety Science*, Hemisphere, New York, 129-148 (1989).

27. Yilmaz, A., Radiation Transport Measurements in Methanol Pool Fires with Fourier Transform Infrared Spectroscopy, NIST Grant/Contractor Report GCR 09-922, January 2009.

28. Mandin, P., and Most J-M., Characterization of the Puffing Frequency on a Pool Fire, *Proceedings of the Sixth International Symposium on Fire Safety Science*, 1137-1148 (2000). doi:10.3801/IAFSS.FSS.6-1137